Incorporation of Transition-Metal Complexes in Functionalized Mesoporous Silica and Their Activity toward the Oxidation of Aromatic Amines

ARTICLE *in* THE JOURNAL OF PHYSICAL CHEMISTRY B · OCTOBER 2000

Impact Factor: 3.3 · DOI: 10.1021/jp000564p

4 AUTHORS, INCLUDING:

Ahmed Zaki
Tanta University
42 PUBLICATIONS **763** CITATIONS
SEE PROFILE

Mohamed Y E-Sheikh
Tanta University
31 PUBLICATIONS **274** CITATIONS
SEE PROFILE

Sherif El-Safty
National Institute for Materials Science
168 PUBLICATIONS **3,239** CITATIONS
SEE PROFILE

Incorporation of Transition-Metal Complexes in Functionalized Mesoporous Silica and Their Activity toward the Oxidation of Aromatic Amines

J. Evans,*,† A. B. Zaki,‡ M. Y. El-Sheikh,‡ and S. A. El-Safty‡

Department of Chemistry, University of Southampton, S017 1BJ, UK, and Department of Chemistry, Faculty of Science, Tanta University, Tanta, Egypt

Received: February 11, 2000; In Final Form: August 14, 2000

The highly ordered mesoporous material H_ISiO_2 was prepared at room temperature and low pH utilizing a high concentration of nonionic surfactant to achieve a hexagonal ordered phase with a pore size of ∼3.5 nm. The grafted amino ligand was covalently bonded to the internal pore surface of H_ISiO_2 through a silanation procedure. Thereby, immobilized transition-metal−aquo complexes such as Mn^{II}−aquo (**I**), Cu^{II}−aquo (**II**), Co^{II}−aquo (**III**), and Zn^{II}−aquo (**IV**) were coordinated to the supported wall without impregnation on the surface. Diffuse reflectance spectroscopy (DRS) and electron paramagnetic resonance (EPR) studies observed that a proportion of the Mn^{II} complex was oxidized to a higher oxidation state, particularly Mn^{IV}. The kinetics and mechanism of redox reactions between *o*-aminophenol, *o*-phenylenediamine, and *p*-pheneylenediamine and the incorporated transition-metal−aquo−propylamine complexes have been investigated. The oxidation products of the amines have been monitored by UV−vis spectroscopy. The reaction follows first-order kinetics, and the rate constant of the oxidation of amines decreases in the following order: $Mn^{IV}/Mn^{II} \rightarrow Cu^{II} \rightarrow Co^{II} \rightarrow Zn^{II}$. This trend is attributed to the reduction potential of the metal ions in the reaction medium. The most obvious feature of the oxidation reaction of amines with complexes **III** and **IV** is that there is a well-defined induction time, whose rate depends on the reactivity and the initial concentration of these amines, prior to a rapid growth in the production of the oxidation product of amines. The experimental results indicate that the outer-sphere mechanism is probably followed in this redox system. Extensive studies of the transition-metal complexes on H_ISiO_2 have been conducted before and after the redox reaction by a wide variety of characterization techniques which include powder X-ray diffraction, DRS, the Brunauer−Emmett−Teller method for nitrogen adsorption and surface area measurements, NMR, EPR, and IR.

Introduction

The transition-metal−amine complexes are of special interest because they show activity against cisplatin (antitumor drug)-resistant cell lines[1−4] and the ability to form dioxygen adducts reversibly,[5] which can be used in biologically active reactions. The intramolecular oxidation of amines to imines by metal ions coordinated to amines has been reported with iron,[6,7] copper,[8] nickel,[9,10] ruthenium,[11,12] and platinum.[13] The oxidation products of aromatic amines used in this work, which are all well-known phenoxozine compounds,[14−16] have attracted considerable attention since the discovery of cancer. Phenoxozine is related to the naturally occurring antibiotic actinomycin D[17,18] that is used clinically for the treatment of certain types of cancer.[19] In the redox reaction between *p*-phenylenediamine and Ag^I,[20−23] an induction period was apparent and dependent on pH and the concentration of amine, not on the reactant concentration. The oxidation mechanism of aromatic amines has been investigated elsewhere.[24−27]

Mesoporous silica MCM-41[28,29] and FSM-16[30−32] with high surface area, narrow pore size distribution, and high thermal stability have attracted considerable attention in recent years, particularly in oil refining and petrochemistry,[33−35] optics,[36] conductors,[37] and electronic devices.[38,39] Typically, these materials are synthesized at relatively high temperatures through the direct condensation of silanol groups in the presence of cationic surfactants (S^+), namely, alkyltrimethylammonium salts, and anionic inorganic species (I^-), (S^+I^-). The main difference between the previous materials MCM-41 and FSM-16 is in the synthesis procedure and formation mechanism. However, an intermediate lamellar silica surfactant was observed during the synthesis of FSM-16, whereas no intermediate phases were observed during the formation of MCM-41.[40] Further investigation with cationic surfactants, in acidic media, designated the key interactions as ($S^+X^-I^+$), where $X^- = Cl^-$ or Br^-.[41,42] On the other hand, the (S^-I^+) pathway involves the condensation of inorganic species in the presence of an anionic surfactant. In the case of the anionic inorganic species and surfactant, the intermediate phase was formed by a small cationic metal (M^+) with the opposing charges ($S^-M^+I^-$), where $M^+ = Na^+$ or K^+.[41,42]

Hexagonal mesoporous silica (HMS) was produced by a low concentration of the neutral template; according to the route (S^0I^0), a wormlike disordered mesoporous silica in neutral media is assembled by hydrogen bonding.[43−45] This interaction allows the organic phase to be totally removed by solvent extraction from the as-synthesized material. The absence of the 110 and 200 reflections in the X-ray patterns indicates only short-range hexagonal order compared with that of FSM-16 and MCM-41.[43] Improvements of the synthesis of the ordered HMS materials have been reported by using nonionic surfactants in the presence of fluoride anions under near-neutral conditions,

* To whom correspondence should be addressed at the Chemistry Department, University of Southampton, Southampton S017 1BJ, U.K. E-mail: je@soton.ac.uk.

† University of Southampton.

‡ Tanta University.

10.1021/jp000564p CCC: $19.00
Published on Web 10/19/2000

where F^- ions are coordinated to silica intermediates (S^0H^+) (F^-I^0).[46] In addition, the synthesis in acidic media was investigated via the (S^0H^+) (X^-I^0) route.[47,48]

A recent advanced approach to form highly ordered mesoporous materials (H_I-silica) has been reported by Attard et al.[49] In this approach, a higher surfactant concentration is used to generate a homogeneous liquid crystalline phase according to the phase diagram of the surfactant−water mixture. Even though this route is independent of the structure of and charge on the surfactant, the mesoporous materials from nonionic surfactants yield structures as equally well-ordered as those from ionic ones. Furthermore, the crystalline H_I-silica that is formed typically has higher pore and particle size dimensions than the powdered MCM-41 materials.

The modification of mesoporous materials by grafting metal complexes is an important area of research in heterogeneous catalysis. One of the best pathways has already been achieved by anchorage of a neutral ligand onto silica through covalent Si−O−Si bonds.[50−55] The neutral ligands were mainly amine or phosphine functions directly grafted to the silica surface by a silanation procedure. These types of ligands permit immobilization of metal complexes, through a coordination bond with metal centers.

Brunel and co-workers[56−58] have used 3-aminopropyl- and 3-chloropropyltriethoxysilane as intermediates for grafting amino functionality and functionalized alkoxysilanes to MCM-41. By a similar methodology, manganese(III) Schiff base complexes were added to modified MCM-41.[58]

The immobilization of cobalt chelate complexes onto MCM-41 was performed through methoxysilyl coupling agents functionalized with ethylenediamine (ED), diethylenetriamine (DET), and ethylenediaminetriacetic acid salt (EDT).[59] The resulting materials showed some reactivity toward forming oxygen adducts. FSM-type mesoporous silicas with different densities of silanol groups have been silylated using chloroalkyldimethylsilane and aminopropylethoxysilanes.[60] In addition, HMS has been grafted with amines by using dimethylaminopropyl groups.[61] The prepared materials show high activities toward Michael addition reactions.

Our goal in this research focuses on creating a highly ordered hexagonal mesoporous silica (H_ISiO_2) using nonionic surfactant Brij 76 by the Attard route.[49] Then, immobilization of the transition-metal−aquo complexes onto functionalized amino-H_ISiO_2 to form stable complexes on the walls of silica is targeted. A thorough study of the kinetics and mechanism of the amine oxidation by the resulting materials has been conducted.

Experimental Section

Materials. 3-Aminopropyltriethoxysilane and tetramethyl orthosilicate (TMOS) were obtained from Fluka. Brij 76 (polyethylene(10) stearyl ether), amines such as *o*-aminophenol (*o*-AP), *o*-phenylenediamine (*o*-PDA), and *p*-phenylenediamine (*p*-PDA), and transition-metal salts such as cupric nitrate trihydrate, manganese(II) nitrate hexahydrate, cobalt(II) nitrate hexahydrate, and zinc nitrate hexahydrate were all supplied by Sigma-Aldrich Co. Ltd., U.K. The stock solutions of the amines (0.01 M) that were prepared in an ethanol−water mixture, 10% for *o*-AP and 20% for both *o*- and *p*-PDA, were diluted to obtain the suitable concentration of the amine. In all cases, the percentage of ethanol is not more than 2% in the amine solution during the redox reactions of all the amines. All the transition-metal salts were dissolved in water to form the aqo complexes.

Preparation of H_ISiO_2. H_ISiO_2 was prepared by using the Attard[49] route, with slight variations in procedure depending on the surfactant (Brij 76). Brij 76 was dissolved with agitation in TMOS until homogeneous. HCl (diluted to pH 1.3 with deionized water) was added quickly. The ratio (w/w) surfactant: TMOS:HCl was 1:2:1. The methanol produced from the hydrolysis of the TMOS was removed in vacuo at room temperature. After 10 min, the viscous glassy material was collected and left at 40 °C for 16 h. The surfactant was then removed by calcination at 470 °C (4 h under nitrogen and 14 h under oxygen).

Silylation of H_ISiO_2. The anchoring of 3-aminopropylsilyl groups onto H_ISiO_2 was achieved by addition of 3-aminopropyltriethoxysilane to a suspension of freshly activated H_ISiO_2 in refluxing toluene, with stirring, for 3 h. The ratio was 1:1:20, respectively. The ethanol produced was removed by distillation from the toluene azeotrope. The modified solid (H_ISiO_2–NH_2) was filtered, washed in a Soxhlet apparatus with diethyl ether and dichloromethane, and then dried at 120 °C.

Modification of (H_ISiO_2–NH_2) by Metal−Aquo Complexes. The formation of metal−propylamine−aquo complexes on H_ISiO_2 was carried out by modification of H_ISiO_2–NH_2 (5 g) with metal−aquo complexes (20 mmol = C_0) under nitrogen at room temperature. After 24 h, the supported solid was collected by suction and washed with deionized water. The filtrate concentration of the metal−aquo complex was determined by UV−vis absorption (C_1). From the difference $C_0 - C_1$, the amount per gram of the supported metal complexes on the H_ISiO_2 was determined and was in the range $(2.0-2.4) \times 10^{-3}$ mol/g for all metal complexes.

Additionally, the stoichiometry and the stability constants of the metal−propylamine−aquo complexes were determined by Job's method in the solution. All the complexes have a stoichiometry of 1:2 except complex **IV** (1:1). The stability constants for complexes **I**, **II**, **III**, and **IV** were 732, 140, 204, and 582 L/mol, respectively.

Characterization of the Samples. Powder X-ray diffraction patterns were recorded on a Siemens ($\theta-2\theta$) D5000 diffractometer with monochromated Cu Kα radiation. ^{29}Si MAS was performed for metal-incorporated mesoporous materials on a Bruker AM 300 NMR spectrometer (pulse delay 120 s). The samples were finely ground and loaded into ZrO_2 or SiN rotors and spun at speeds between 3 and 5 kHz. The ^{29}Si chemical shifts are reported relative to tetramethylsilane. Diffuse reflectance spectroscopy (DRS) measurements were recorded on a Perkin-Elmer Lambda 19 UV−vis/near-IR spectrometer. The samples were placed in quartz solid cells, and the spectra were obtained in Kubelka−Munk mode. Electron paramagnetic resonance (EPR) measurements were carried out on a Bruker ECS 106 X-band spectrometer operating at a microwave frequency of ca. 9.35 GHz and a temperature of 298 K. IR spectra were measured by using a Perkin-Elmer FTIR-1710 with Nujol mull in CsI disks, scanned from 4000 to 450 cm^{-1} with resolution 4 cm^{-1} in 0.4 min. Nitrogen adsorption isotherms and surface area measurements were determined following the Brunauer−Emmett−Teller (BET) method at 77 K, the data being collected with a Micrometry GEMINI III 2375 surface area analyzer. The mass spectrometric experiments were recorded on a Micromass Platform quadrupole mass analyzer (Micromass, Tudor Rd., Altrincham, U.K.). APCI (atmospheric pressure chemical ionization) spectra operating conditions were capillary voltage 3.5 kV, HV lens voltage 0 kV, cone voltage 20 V, source temperature 150 °C, probe temperature 450 °C, ES eluent 100% acetonitrile at 200 μL min^{-1}, nitrogen drying gas flow rate 250 L h^{-1}, and APCI sheath gas flow rate 50 L h^{-1}. The spectrophotometric measurements were recorded on a

Perkin-Elmer Lambda 19 UV−vis/near-IR spectrometer, equipped with a temperature controller.

Kinetic Measurements. The heterogeneous redox reaction between the amines (*o*-AP, *o*-PDA, and *p*-PDA) and a known amount of H_ISiO_2 supported with complexes **I**, **II**, **III**, and **IV** was carried out at four temperatures in aqueous−ethanolic solution. The reaction was performed using a water-shaker thermostat; after an interval of time dependent on the nature of the redox reaction, the container was removed from the thermostat and the reaction was quenched quickly by suction. The oxidation product of amines was monitored kinetically by UV−vis spectroscopy.

Results and Discussion

Characteristics of Incorporated H_ISiO_2 with Metal Complexes. *Synthesis of H_ISiO_2.* Our approach is to exploit the use of the nonionic surfactant assembly (Brij 76) as a structure-directing additive to generate H_ISiO_2 from bulk lyotropic mesophases.[49] The hydrolysis of TMOS in the surfactant/water mixture occurs rapidly and yields an isotropic liquid, because of formation of methanol during the hydrolysis step, which then destroys the mesophase. First, to circumvent this, a vacuum is rapidly used to restore the original mesophase. The calcination is performed at a temperature of 470 °C to establish that all the surfactant templates are removed from the synthesis materials and from the H_ISiO_2 materials. In addition, the most significant advantage in the formation of H_ISiO_2 is mainly that the addition of HCl with low pH (1.3) shifts the equilibrium of the condensation process toward the formation of H_ISiO_2.[62] It also assists in causing rapid condensation at room temperature without loss of the long-range order of the hexagonal phase.[63] Second, utilizing the high concentration of Brij 76 (50 wt %) permits a homogeneous liquid crystalline phase. Consequently, the monolithic H_ISiO_2 permits a highly facile quenching process during the heterogeneous redox reaction. Third, the true liquid crystal template mechanism is described for the formation of H_ISiO_2 with Brij 76. However, the precursor of the hexagonal liquid crystal mesophase (H_I) aggregates to form cylindrical hexagonal rods, packing together with hexagonal symmetry. Subsequently, the polycondensation process permits the formation of the silicate species around the hexagonal phase.[64]

BET Measurements. According to the nitrogen BET adsorption measurements, the specific surface area of the calcined H_ISiO_2 was found to be 760 m^2/g. This value reflects a high internal surface area of the mesoporous framework. Nitrogen adsorption/desorption curves displayed no hysteresis (Figure 1a), suggesting that there is a highly uniform pore size with no obstruction of narrow pores during the desorption, and also the framework of silicate is composed of straight channels without any intersecting zigzag channels.[65,66] The pore size distribution curve (Figure 1b), which was obtained from the desorption data, shows a peak at 3.5 nm, indicating that H_ISiO_2 has well-defined uniform pore dimensions.[49] Generally, this result indicates a high-quality support for both the anchorage of metal complexes to the internal surface area without changing the regularity or structure of H_ISiO_2 and also fast diffusion of amines during the redox reaction.

Powder X-ray Diffraction (PXRD) Studies. Calcination at 470 °C yields a well-resolved PXRD pattern (Figure 2a). Long-range hexagonal order and a high crystallinity of H_ISiO_2 were observed, as indicated by the presence of d_{100}, d_{110}, and d_{200} reflections.[67] The PXRD of H_ISiO_2 displays a d_{100} spacing of ≅4.9 nm, which is similar to that reported for the silicate−surfactant lyotropic liquid crystal phase.[68] Such PXRD patterns

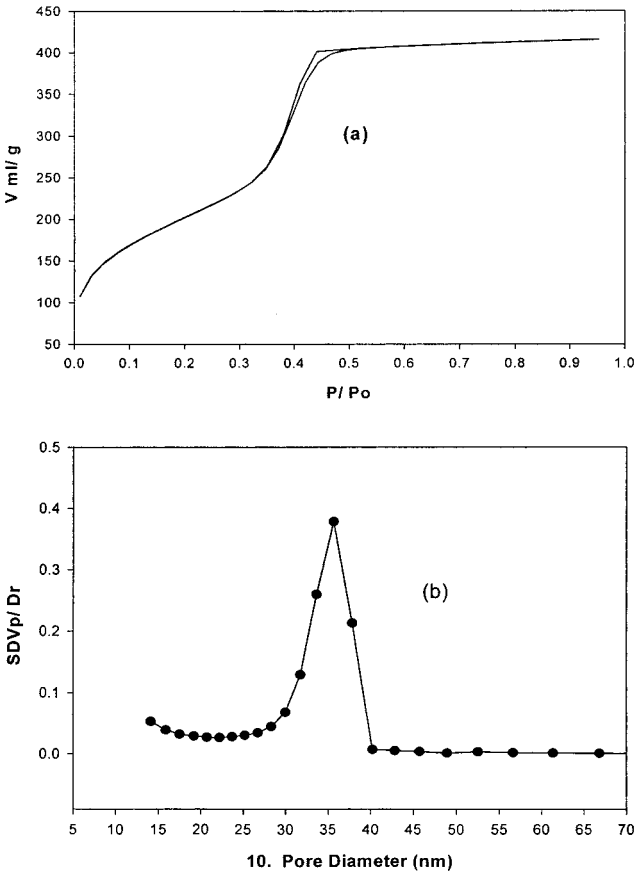

Figure 1. (a) Nitrogen adsorption−desorption isotherms for H_ISiO_2 (the relative pressure is p/p_o, where p is the equilibrium pressure of the adsorbate and p_o is the saturation pressure of the adsorbate at the temperature of the adsorbent; V is the volume adsorbed at STP). (b) The corresponding Horvath−Kawazoe plot for the adsorption data (dv/dr is the derivative of the nitrogen volume adsorbed with respect to the pore diameter of the adsorbent).

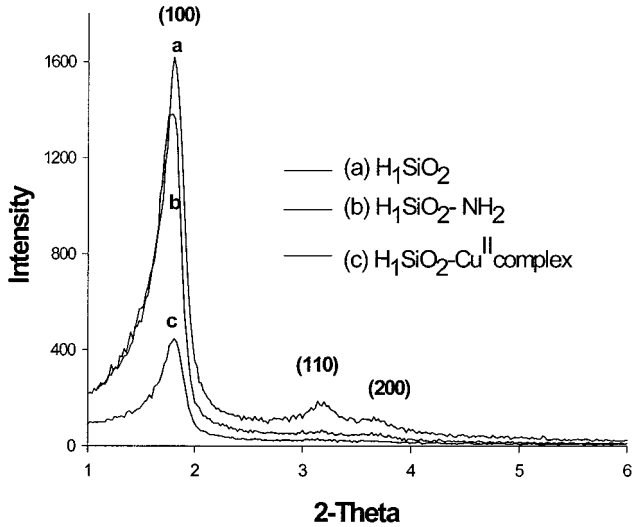

Figure 2. PXRD patterns of (a) calcined H_ISiO_2, (b) functionalized propylamine−silane−H_ISiO_2 (H_ISiO_2−NH_2), and (c) the incorporated Cu^{II}−aquo complex (H_ISiO_2−NH_2/Cu^{II}).

that exhibit strong 100 reflections and several low-order weak reflections are usually observed in mesoporous material such as HMS,[43] MCM-41,[28,29] and FSM-16.[31,32]

Significant features evident from Figure 2b,c follow: first, the broadening of the peaks of the d_{100} reflection after the functionalization steps is apparent, because of the reduction of

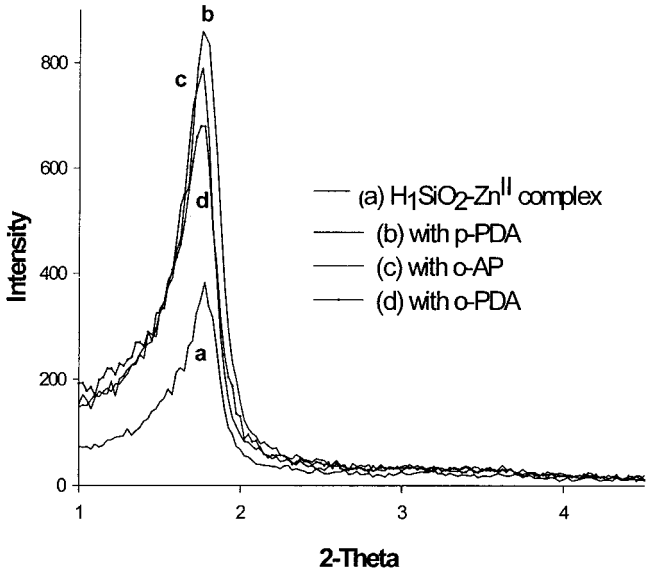

Figure 3. PXRD patterns of (a) the H_ISiO_2/Zn^{II} complex and (b−d) the H_1SiO_2/Zn^{II} complex after redox reaction with *p*-PDA, *o*-AP, and *o*-PDA.

the order of silanol Si−OH groups via ethanolic elimination and the decrease of the crystallite mosaic size.[69] Second, after the metal complexes are grafted onto the meso structure, the 2θ values of the d_{100} peaks of the materials are extremely similar. This phenomenon indicates that the mesoporous architecture of the support is structurally unchanged and the metal complexes II, **III**, **IV**, and **I** are well dispersed inside the channel pores. Third, the decrease in the intensity of the 100 reflection peak may be assigned to the partial structure collapse of the ordered hexagonal phase, or the flexibility of the silica framework resulting from the strain of the incorporated metal complex.[70]

Moreover, PXRD patterns of the incorporated metal complexes on H_ISiO_2 showed that the intensity of the 100 reflection peak after the redox reaction (Figure 3) is clearly increased in line with the reactivity of the amines toward the metal complexes. In other words, the intensity is proportional to the rate of the amine oxidation, which increases in the order *o*-PDA < *o*-AP < *p*-PDA. These results may indicate that the redox reaction relieves the distortion on the texture of H_ISiO_2 through the formation of new configurations of the reduction form of metal complexes.

^{29}Si MAS NMR Studies. The structures of the H_ISiO_2 materials and the amine-functionalized H_ISiO_2 materials and the chemical bonding can be studied by solid-state NMR experiments (Figure 4). The ^{29}Si NMR spectra of H_ISiO_2 show three overlapping broad resonances between −90 and −120 ppm. The broad resonance is indicative of a wide range of Si−O−Si bond angles and formation of a multiple tetrahedral silicon environment[71] (Figure 4a). Isolated $Si(OSi)_4$ (Q_4) sites are evident at δ −113 ppm, where $Q_n = Si(-OSi-)_n(OH)_{4-n}$. The ^{29}Si shoulder peaks at δ −91 and −100 are assigned to the central Si atom in $Si(OSi)_2(OH)_2$ (Q_2) and $Si(OSi)_3(OH)$ (Q_3) sites, respectively.[72] However, the Q_3:Q_4 ratio in these MAS NMR experiments is somewhat indistinct.

Furthermore, Figure 4b,c represents the ^{29}Si NMR spectra of H_ISiO_2 after silanation of propylamine−silane and immobilization of metal complexes, respectively. Whereas the large peak at −113 ppm is from the silica framework, the two additional peaks between −50 and −80 ppm, observed in Figure 4b,c are due to two different environments for the siloxane group in the incorporated monolayers.[73] The ^{29}Si peaks at −63 and

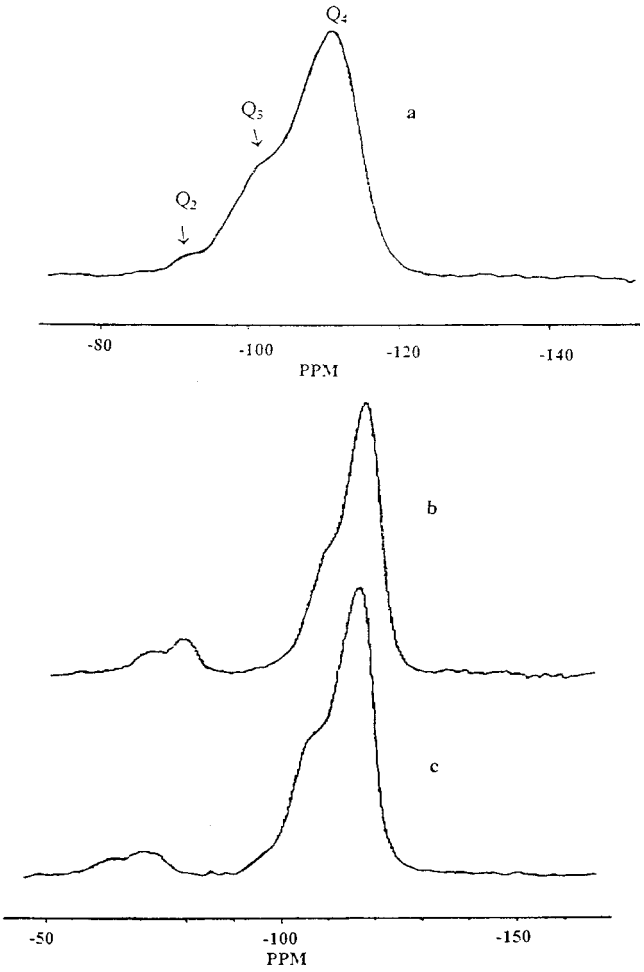

Figure 4. ^{29}Si MAS NMR spectra of (a) calcined H_ISiO_2 (b) functionalized H_ISiO_2–NH_2, and (c) the H_ISiO_2/Co^{II} complex.

−72 ppm correspond to the $H_2NCH_2CH_2CH_2Si(OX)_3$ groups that are bound to two and three neighboring siloxanes (X = Si), respectively. Figure 4b,c shows that the latter groups are the most predominant species, which are mainly assigned to the aminosilane bound to triplet surface hydroxyl groups.[74] Additionally, the functionalized aminosilane has formed at least one chemical bond with surface siloxane in the reaction phase. The interaction has occurred via the ethanol leaching to form Si−O−Si and not through the formation of the hydrogen bond between the amino and surface hydroxyl groups.[75] This conclusion was confirmed with the formation of the propylamine complexes and the stability of these complexes during the redox reaction, where the ^{29}Si NMR peaks after the redox reaction are exactly the same (Figure 4c).

IR Spectroscopy. In situ IR spectroscopic studies further confirm that (i) true chemical interaction has occurred when H_ISiO_2 is treated with 3-aminopropyltriethoxysilane, (ii) the aminosilane has reacted with hydroxyl groups on the H_ISiO_2 support, and (iii) the stability of immobilized complexes has been achieved on H_ISiO_2, as shown in Scheme 1. Figure 5 shows the IR spectra of H_ISiO_2 as well as its modification with an NH_2 group and metal complexes. It is worth noting that the signal at 3746 cm^{-1}, which is attributed to isolated surface silanol groups, completely disappears and the band corresponding to the NH_2 deformation frequency is also observed at 1630 cm^{-1}.[76] This is good evidence that the complete elimination of the ethoxy groups to form stable covalent bonds with the framework of H_ISiO_2 has occurred.[77,78] Simultaneously, the band

SCHEME 1: Simplified Model of the Surface Sites in the Functionalized Silicas and Immobilized Complexes[a]

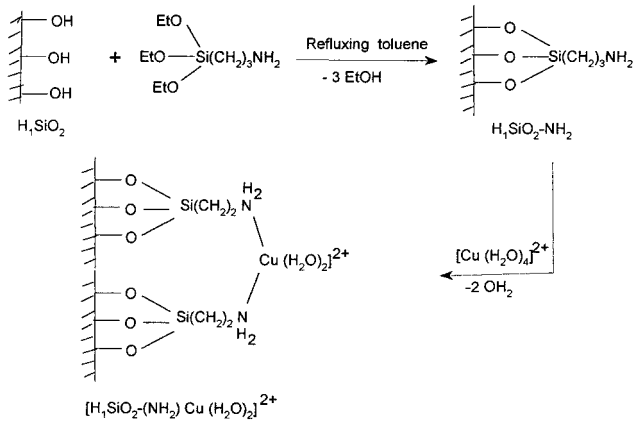

[a] Only one of the mixtures of $NH_2(CH_2)_3Si(OX)_3$ groups is shown.

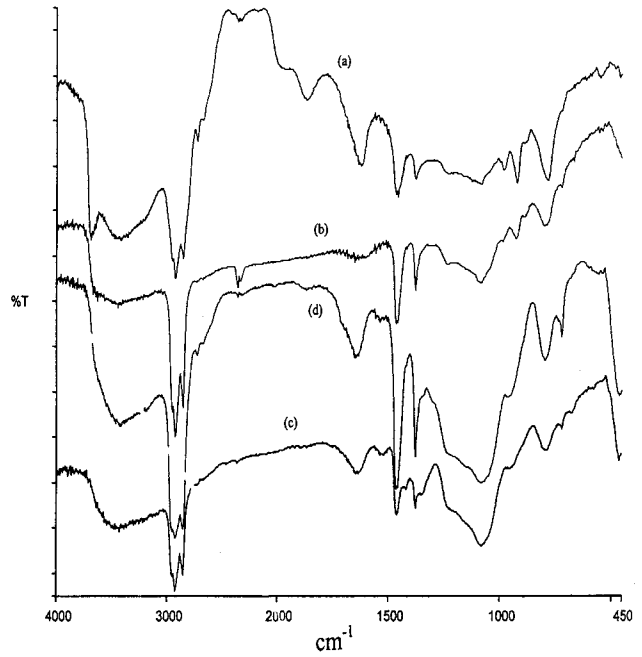

Figure 5. IR spectra of (a) H_ISiO_2, (b) H_ISiO_2–NH_2, and (c, d) the H_ISiO_2/Zn^{II} complex before and after the redox reaction, respectively (Nujol mull with CsI disks).

at 1070 cm^{-1} indicates the presence of Si−C bonds in the Si−O−Si stretching region.[70] Figure 5c shows that the metal complex coordinates with the amino group. This confirms that the interaction between the grafted ligand and the silicate support has been achieved via the condensation of ethoxy groups to produce ethanol, not through the hydrogen bond between NH_2 and the Si−OH surface. Additionally, Figure 5d shows that the metal complexes incorporated onto H_ISiO_2 are stable during redox reaction and exist in the pore channel without any extraction.

Diffuse Reflectance Spectroscopy. DRS studies were concerned with investigating the structure of the immobilized complex and providing good evidence about incorporation into the H_ISiO_2. However, the UV−vis region of the DRS spectra shows the aminosilane absorption band at λ 300 nm after immobilization of H_ISiO_2 by amino groups (Figure 6A(a,b)). The treatment of the metal−aquo complexes (Mn^{II}, Co^{II}, Cu^{II}, and Zn^{II}) with the functionalized amino-H_ISiO_2 occurred in aqueous solution under nitrogen to avoid the effect of oxygen. The change in color of (H_ISiO_2–NH_2) is itself a good indication

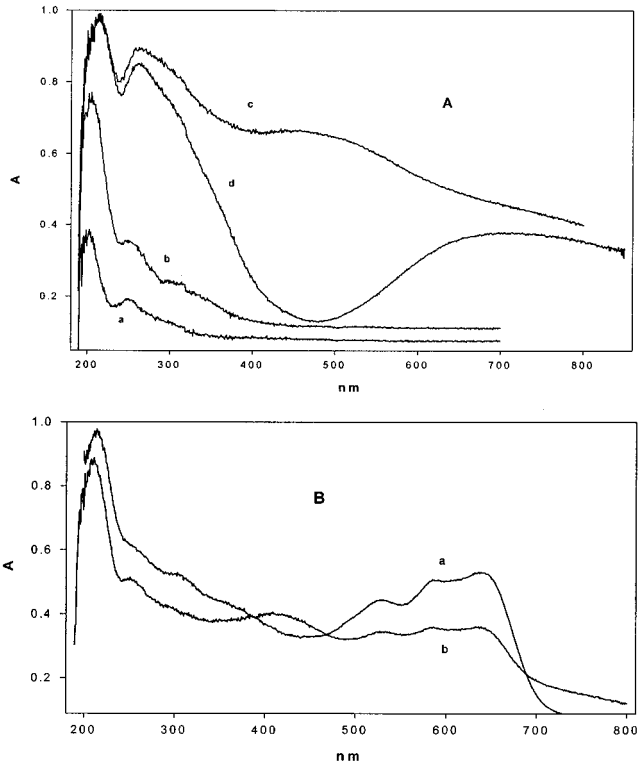

Figure 6. (A) Diffuse reflectance spectra of (a) calcined H_ISiO_2, (b) H_ISiO_2−NH_2, (c) the H_ISiO_2/manganese complex, and (d) the H_ISiO_2/Cu^{II} complex. (B) Diffuse reflectance spectra of the H_ISiO_2/Co^{II} complex (a) before and (b) after redox reaction with *o*-PDA.

that the metals are coordinated by the grafted ligand. For the Mn^{II} complex, after the sample has been freshly dried, DRS exhibits a band at 450 nm (Figure 6A(c)), even though the transitions of Mn^{2+} are all spin forbidden and as a consequence very weak. However, the d−d transitions of Mn^{3+} and Mn^{4+} can be seen.[79,80] This means that part of the manganese has been oxidized to higher oxidation states (Mn^{3+} and Mn^{4+}). But DRS cannot differentiate which oxidation states are present with Mn^{2+}. As shown in Figure 6A(d) for the Cu^{II}−propylamine−aquo complex/H_ISiO_2, the extensive and wide band at λ ca. 690 nm is attributed to the formation of $[Cu(propylamine)_2(H_2O)_2]^{2+}$.[81] With respect to the UV−vis absorption spectra of the Zn^{II} complex, there are no clear spectral changes compared with the functionalized amino group with H_ISiO_2 spectra.

The DRS spectra of H_ISiO_2 with the Co^{II}−propylamine−aquo complex (Figure 6B(a)) displayed a broad band between 500 and 700 nm with splitting into triplet bands at λ values of 520, 580, and 650 nm. This is due to spin−orbit coupling, and the triplet bands are due to a high tetrahedral symmetry of the Co^{II} complex.[81]

After the redox reaction between the amine (*o*-PDA) and the Co^{II} complex/H_ISiO_2, as shown in Figure 6B(b), the intensity of the absorption band of the characterized metal complex/H_ISiO_2 decreased and a new band at λ 420 nm appeared with *o*-PDA oxidation. This may be attributed to the reduction of the metal ions in the redox system and strong adsorption of the oxidation product on the H_ISiO_2 after reaction.

Electron Paramagnetic Resonance Spectroscopy. EPR studies were used to characterize the metal ions in the mesoporous silica before and after the oxidation reaction of amines. EPR spectra of the Mn^{II} complexes in functionalized H_ISiO_2 are shown in Figure 7a. At 298 K, six well-resolved hyperfine lines centered at $g = 1.96$ and a hyperfine splitting constant $A = 85$ G are observed, characteristic of a manganese complex in octahedral

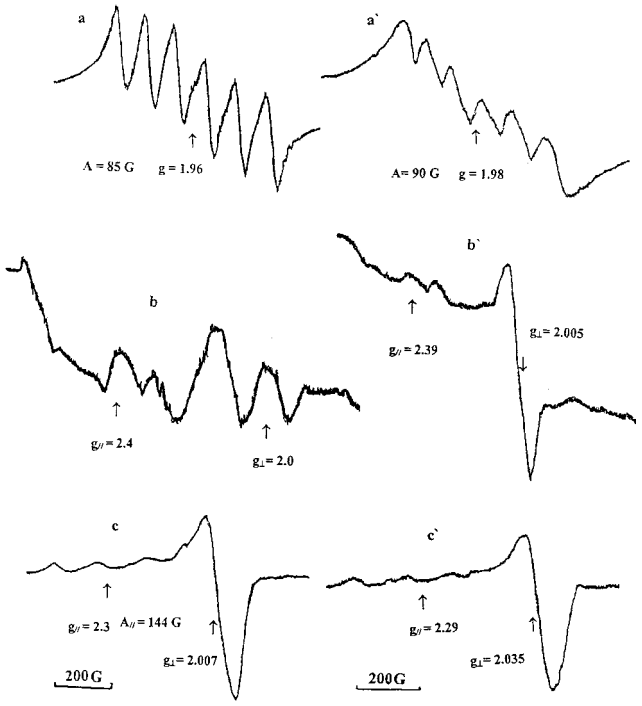

Figure 7. EPR spectra of H_ISiO_2/manganese−H_ISiO_2/Co^{II}−propylamine−aquo, and H_ISiO_2/Cu^{II}−propylamine−aquo complexes (a−c) before and (a′−c′) after the redox reaction with amines, respectively.

coordination, as seen by various authors.[82,83] The equality of the sextet lines of Mn^{2+} in spacing and line height is due to zero-field interaction.[82] With the low manganese complex loading (Mn/Si = 2.2×10^{-3} mol/g), the EPR singlet at $g = 1.96$ with $A = 85$ G indicates that part of the Mn^{2+} was oxidized to Mn^{4+}, not to Mn^{3+}, since the X-band EPR spectra exhibit no signal for Mn^{3+}.[84] Consequently, both Mn^{2+} and Mn^{4+} complex cations must be present in the anchoring of the manganese complex.[85] As a result of the redox reaction, the Mn^{4+} was reduced to Mn^{2+}. Therefore, the broad wings of the sextet spectra are observed with $g = 1.98$ and $A = 90$ G (Figure 7a`), due to the increasing spin interaction with a high concentration loading of Mn^{2+}.[86]

In the case of the Co^{II}−propylamine−aquo complex impregnated onto H_ISiO_2 (Figure 7b), the EPR spectrum has been assigned to high-spin Co^{II}.[87] Two main signals are observed at $g_{||} = 2.4$ and $g_2 \approx g_3 = g_\perp = 2.0$. It is known that the signal at $g = 2$ represents a highly symmetric tetrahedral environment.[87] The broadened spectra are probably due to the differences in the relaxation parameters and the spin−spin interaction between the adsorbed metal ions.[88] After the redox reaction, the intensity of the signal at $g_{||}$ is considerably reduced by more than 20 times (Figure 7b). On the other hand, the sharp band at $g_\perp = 2.005$ appears instead of g_2 and g_3, which may indicate radical formation during the redox reaction.

The Cu^{II} ion EPR spectrum of Cu^{II} complex/H_ISiO_2 can be fundamentally described by an axial spin Hamiltonian with $g_{||}$ and $g_\perp$, which are split into quartets due to hyperfine interaction between the unpaired electron and copper nuclei (^{63}Cu and ^{65}Cu nuclei with a nuclear spin of 3/2) (Figure 7c).[89] The intensity of the $g_{||}$ and $g_\perp$ signals being only 3 and 20, respectively, indicates the weakness of the signal because of the instrumental noise level. The parameters $g_{||} = 2.3$, $g_\perp = 2.007$, and $A_{||} = 144$ G are observed. After the redox reaction, the EPR signal of $g_\perp$ is characterized by weaker signals and a broadened line width, which is mainly due to the electron spin−spin interactions

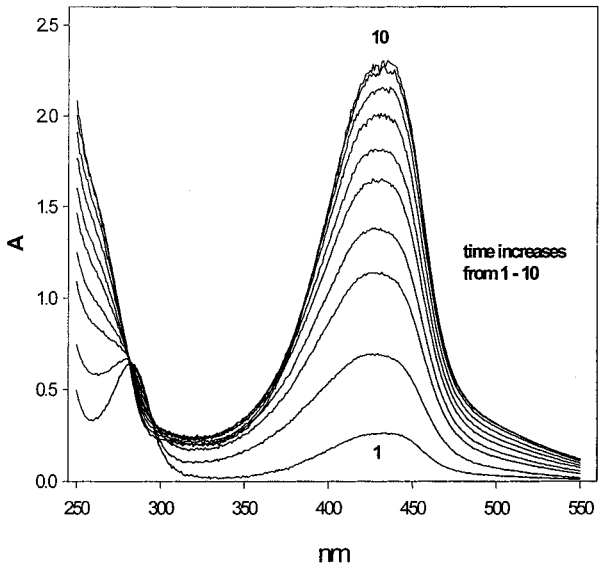

Figure 8. Time sequence of the increase in the absorption band of the oxidation product of *o*-aminophenol (2.1×10^{-4} M) for the redox reaction with H_ISiO_2/metal complexes.

(Figure 7c`). This is evidence that part of the Cu^{II} is being reduced to Cu^{I}. Furthermore, the hyperfine lines on the perpendicular component are still visible, even though less resolved than in spectrum a. No coupling to an isotropic spin was observed on the signal, and still the spectra can be described by the parameters $g_{||} = 2.29$ and $g_\perp = 2.035$.

With respect to Zn^{II} complex/H_1SiO_2, it is nearly impossible to obtain any EPR spectrum because the Zn^{II} ion is EPR silent.

Kinetic Study of the Redox Reactions. *Rate of Redox Reactions*. The redox reactions occur between the amines (*o*-AP, *o*-PDA, and *p*-PDA) and the immobilized H_ISiO_2 with metal ion complexes **I**, **II**, **III**, and **IV** under ambient conditions. The oxidation product of the amines was monitored kinetically by UV−vis absorption at 435 nm for *o*-AP and 420 nm for *o*-PDA,[90,91] as shown in Figure 8. But with *p*-PDA it was monitored at 510 nm[92] in the case of complexes **II** and **IV** and at 450 nm for the others.[93]

For all redox reactions, the first-order kinetics is followed according to the following equation:[94]

$$\ln \frac{A_f}{A_f - A_t} = kwt$$

where A_f is the absorbance at infinite time, A_t is the absorbance at time t, w is the amount (g) of supported H_ISiO_2, and k is the observed rate constant. The true rate constant, k_t, per gram of support (pgs), which is only temperature dependent, was determined and is summarized in Table 1.

The most obvious feature of this redox reaction is that an induction period was observed with the oxidation of all amines by complexes **III** and **IV** (Figure 9). It was found that the temperature did not affect the well-defined induction period for all amines (Figure 10). On the contrary, the induction period gradually disappeared when the amine concentration was increased and completely vanished at [amine] = 6.3×10^{-4} M[95,96] (Figure 11).

Our experiments showed that the induction time, which appeared in the redox reactions of the both complexes **III** and **IV**, is inversely related to the reactivity of the amines (Figure 12). This means that the oxidation reaction rate of the amines is mainly affected by the apparent induction period.

TABLE 1: Illustration of the Rate Constant k_t (pgs) and the Activation Parameters of the Redox Reaction of Amine A (2.1×10^{-4} M) with Transition-Metal−Propylamine−Aquo Complexes Supported on H_ISiO_2

		$10^5 k_t$,[a] s^{-1}, at T, °C								
complex	[A]	25	30	35	40	45	E, kJ/mol	$\Delta H^{\ddagger}$, kJ/mol	$\Delta G^{\ddagger}$, kJ/mol	$\Delta S^{\ddagger}$, (J/mol)/deg
I	*o*-AP	78.0	103.0	146.5	200.5		50.1(2)	47.56	91.65	144.3(7)
	o-PDA	67.7	86.3	105.0	134.0		36.0(1)	33.46	93.00	195.0(4)
	p-PDA	226.0	302.1	442.0	815.0		66.5(7)	63.96	88.60	81(2)
II	*o*-AP	17.6	22.43	27.5	33.3		33.6(3)	31.1	96.00	212.0(9)
	o-PDA	5.00	6.50	8.04	9.62		36.0(3)	33.5	98.03	211(1)
	p-PDA	29.9	36.7	44.33	53.7		30.0(1)	27.7	93.90	217.0(5)
III	*o*-AP	8.33	11.2	14.9	28.75		41.0(5)	38.5	97.53	193(2)
	o-PDA	2.64	4.10	5.46	6.54		47.0(9)	44.5	100.2	182(3)
	p-PDA	14.77	18.33	24.5	31.07		36.0(5)	33.5	96.30	206(2)
IV	*o*-AP	3.13	4.03	4.84	5.53		29.1(1)	26.60	100.5	242(2)
	o-PDA		0.96	1.42	2.10	2.78	54.9(3)	52.40	101.6	158(1)
	p-PDA	5.10	5.96	7.30	8.87		27.5(6)	24.96	99.50	243.0(4)

[a] Standard deviations are in the range $(2-10) \times 10^{-2}$ for all rate constants.

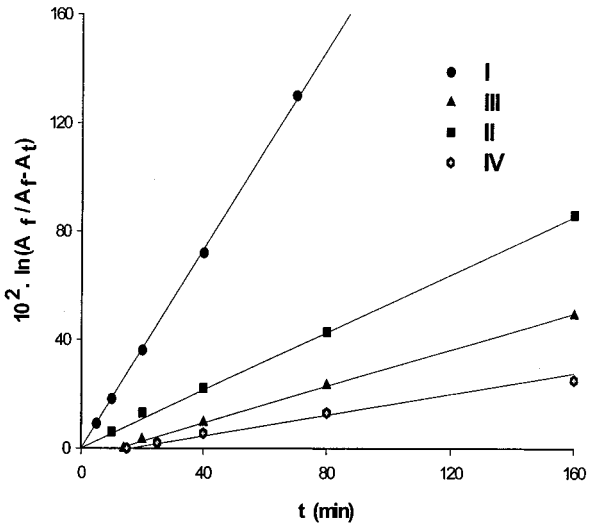

Figure 9. Integrated first-order rate equation of the heterogeneous redox reaction between *o*-aminophenol (2.1×10^{-4} M) and metal−propylamine−aquo complexes supported on calcined H_ISiO_2 at 30 °C.

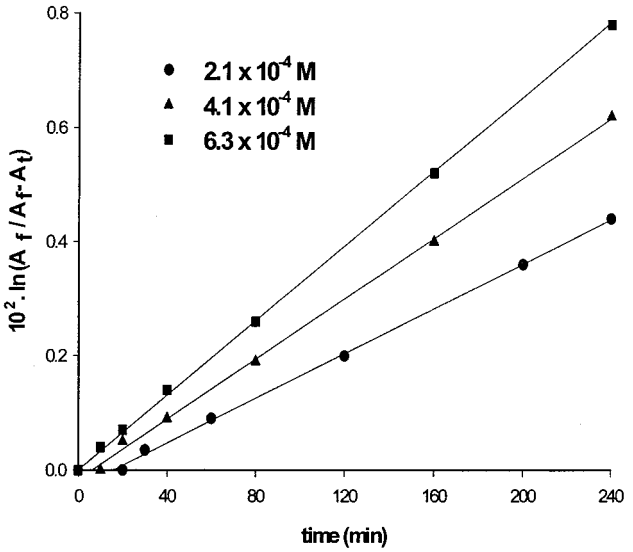

Figure 11. Integrated first-order equation of the redox reaction between Co^{II}− propylamine−aquo complex supported on H_ISiO_2 and *o*-phenylenediamine of different concentrations ($(2.1-6.3) \times 10^{-4}$ M) at 35 °C.

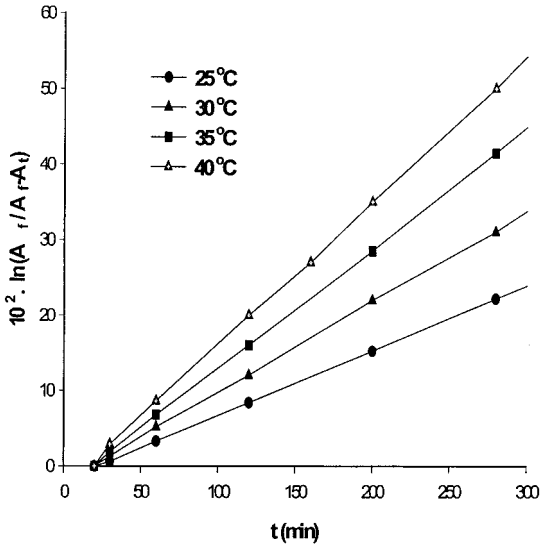

Figure 10. Integrated first-order rate equation of the redox reaction between *o*-phenylenediamine (2.1×10^{-4} M) and the Co^{II}−propylamine−aquo complex supported on calcined H_ISiO_2 at different temperatures.

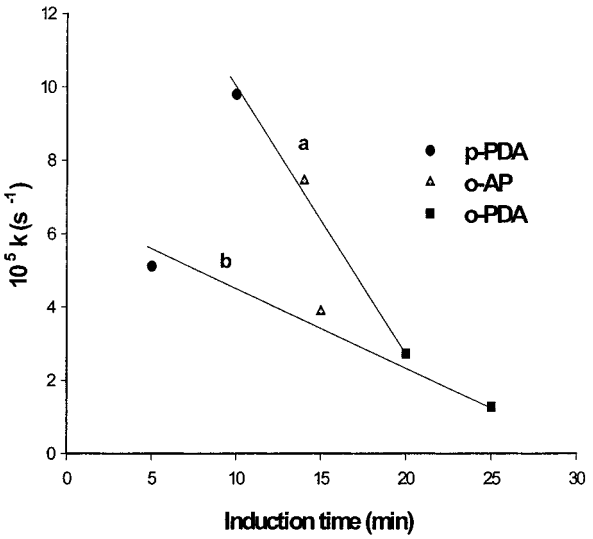

Figure 12. Induction period against the rate constant of the oxidation of amines (2.1×10^{-4} M) with (a) Co^{II}− and (b) Zn^{II}−propylamine−aquo complexes supported on H_ISiO_2 at 35 °C.

From the observed data in Table 1, the k_t value decreased in the order *p*-PDA > *o*-AP > *o*-PDA, which is attributed to variations of the electron density of the amine substituents. This is the same trend as was observed with our previous work carried out on the oxidation of these amines by transition-metal−oxalate complexes in homogeneous and heterogeneous systems.[97]

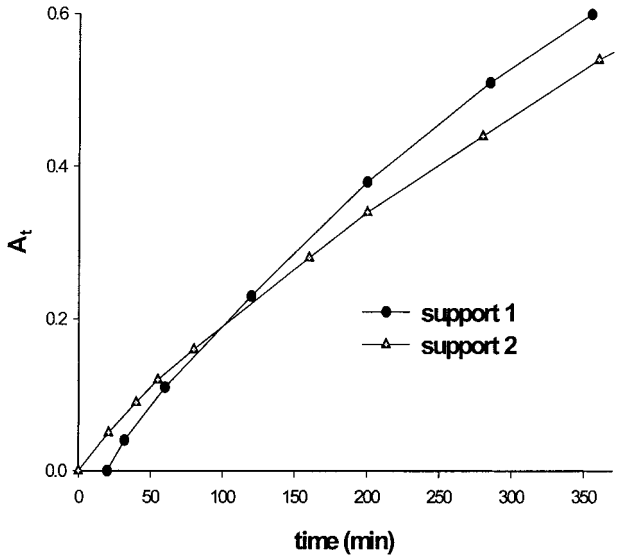

Figure 13. Illustration of the absorbance−time curve of the oxidation product of *o*-phenylenediamine (2.1×10^{-4} M) in redox reaction with the H_lSiO_2/Co^{II-} propylamine−aquo complex (support **1**) and the same complex after the reaction is finished (support **2**) at 40 °C.

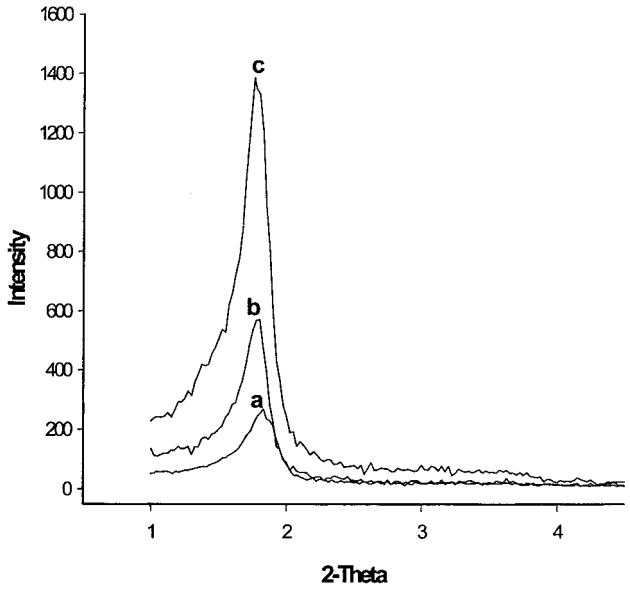

Figure 14. PXRD spectra of the Co^{II-}aquo−propylamine complex supported on H_lSiO_2 (a) before and (b) during the induction time and (c) after the redox reaction with *o*-phenylenediamine (2.1×10^{-4} M).

The oxidation activity of the metal−propylamine−aquo complexes increases in the following order: **IV** < **III** < **II** < **I**. According to the analysis of these complexes by DRS and EPR, part of the Mn^{2+} complex **I** changes to a Mn^{4+} complex during the incorporation process. So, the reduction activity of the metal complexes may be attributed to the effective reduction potential of the metal ion in the reduction medium.[98]

Activation Parameters. The activation energy, *E*, was deduced from an Arrhenius plot. The other activation parameters $\Delta G^{\ddagger}$, $\Delta H^{\ddagger}$, and $\Delta S^{\ddagger}$ were calculated and are listed in Table 1. It can be shown that $\Delta S^{\ddagger}$ and *E* of the amine oxidation reaction with complexes **II**, **III**, and **IV** decrease in the order *o*-PDA > *o*-AP > *p*-PDA. The high negative $\Delta S^{\ddagger}$ value indicates that the transition state is charged and rigid.[99,100] But with complex **I**, $\Delta S^{\ddagger}$ and *E* show the same trend as the rate constant of the oxidation process of these amines.

On the other hand, $\Delta S^{\ddagger}$ and *E* of the redox reaction of the metal complexes with *o*-AP and *p*-PDA increase with the same trend as that of the stability constant of the complexes as follows: **IV** < **II** < **III** < **I**. But with *o*-PDA, the sequence of $\Delta S^{\ddagger}$ and *E* is the inverse of the rate constant of the redox reaction with slight deviation in $\Delta S^{\ddagger}$ of complex **I**.

In addition, the $\Delta G^{\ddagger}$ value is found to be in the 91.6−101.6 kJ/mol range (Table 1). This is the same range found for the oxidation of these amines by Co^{III-}, Mn^{III-}, and Cu^{II-}oxalate complexes supported the Amberlite IRA 904 anion-exchange resin.[97] The value of $\Delta H^{\ddagger}$ is in the range of the chemical reaction control, not the diffusion control.[101] Also, this value shows that the electron-transfer reaction steps may include the substitution reaction process.[102]

Investigation of the Reaction Mechanism. *Reaction Intermediate*. The incorporated H_lSiO_2/metal complexes (support **1**), after use in the oxidation of amines, were collected, washed, and reused in the redox reaction under the same conditions (support **2**). DRS measurements showed that support **2** still had adsorbed amine oxidation product, which is strongly attached to the H_lSiO_2 surface after support **1** is washed. As shown in Figure 13, in the initial stages, the rate of the reaction with support **2** is greater than that with support **1**, and there is no induction period. But with time, the rate using support **2** decreases, suggesting that the adsorbed amine oxidation product shifts the reaction equilibrium toward the reacting species and therefore renders the reaction less facile. These results indicate that an intermediate was formed at the beginning of the redox reaction during the induction period, which had an inhibiting effect on the reaction rate.[103]

Furthermore, PXRD patterns were recorded for the Co^{II-}-amine−aquo complex supported on H_lSiO_2 during the induction time that appears in the redox reaction (Figure 14). The patterns exhibit increases in the intensity of supported H_lSiO_2 during the induction period, and the increase is even greater after the redox reaction (Figure 14a,b). This indicates that the new configuration of the Co^{II-}amine−aquo complex supported on H_lSiO_2 has occurred in the first approach of amine, causing a redox reaction during the induction period. This result establishes that the redox reaction was performed during the induction period but the observed oxidation product was formed via an intermediate.

Effect of the Addition of Functionalized H_lSiO_2−NH_2. The effect of the amount of added functionalized amino-H_lSiO_2 on the redox reaction is shown in Figure 15). The reaction rate of the amine oxidation increases with the presence of H_lSiO_2−NH_2 in the reaction medium. The addition of this solid base might not be expected to have any direct effect on the metal center ions within the other particles of the functionalized amino-H_lSiO_2. It seems most likely that the additional aminated silica enhances the rate of the redox reactions by acting as a proton sink.

The amine oxidation reactions were also carried out with a supported Ru^{III} species that was also synthesized from aqueous $RuCl_3$ and the aminated H_lSiO_2. The rate constants were found to be 10.9, 42.4, and 97.0×10^{-5} s^{-1} for the oxidation of *o*-PDA, *o*-AP, and *p*-PDA at 40 °C, respectively. These values are intermediate between those of the $Mn^{IV/II}$ and Cu^{II} materials. Normally, the redox reactions of the kinetically inert Ru^{III} centers (t_{2g}^5) follow an outer-sphere mechanism, and this may be anticipated also in this case.[104] Other reports have also indicated that the outer-sphere mechanism is predominant for the oxidation of amines by supported metal complexes.[105] We therefore conclude that such a process describes the rapid initial electron-transfer step in this study.

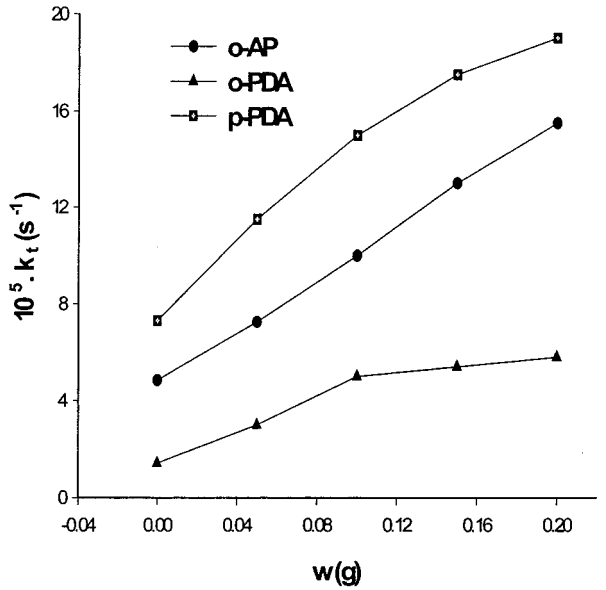

Figure 15. Study of the effect of the addition of different amounts of H_ISiO_2–NH_2 on the rate constant of the redox reaction between amines (2.1×10^{-4} M) and the Zn^{II}–propylamine–aquo complex supported on H_ISiO_2 at 35 °C.

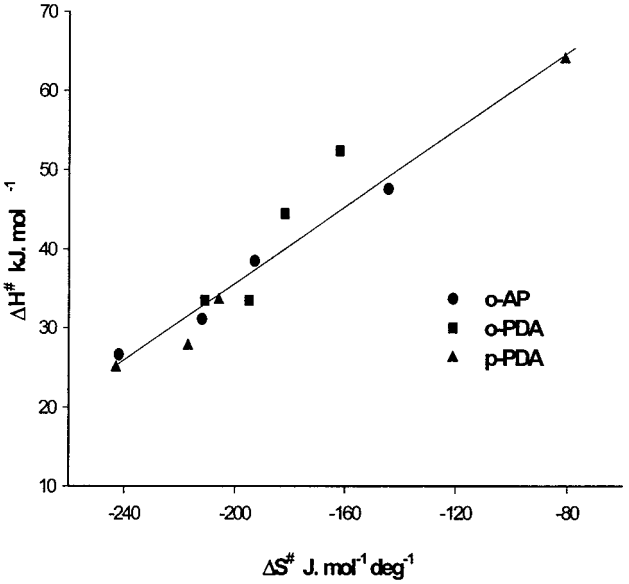

Figure 16. Isokinetic relationship of the redox reaction between amines (2.1×10^{-4} M) and transition-metal–propylamine–aquo complexes supported on H_ISiO_2.

Isokinetic Relationship. The plot of $\Delta H^{\ddagger}$ vs $\Delta S^{\ddagger}$ for the redox reaction gives a straight line (correlation coefficient 0.95) whose slope β (isokinetic temperature) is equal to 253 K (Figure 16). This result provides evidence that the oxidation reaction of amines by supported metal complexes on H_ISiO_2 follows one mechanism. Additionally, the redox reactions are entropy-controlled,[106] which is the same behavior that was found for the oxidation of these amines by Co^{III}–, Mn^{III}–, and Cu^{II}–oxalate complexes supported on Amberlite IRA 904 anion-exchange resin.[97]

Reaction Mechanism. Mass spectrometry (APCI) showed that the oxidation products of *o*-AP, *o*-PDA, and *p*-PDA exhibited a molecular ion consistent with the formation of dimers and a trimer as follows: M = 215, 211, and 319 for the oxidation products of *o*-AP, *o*-PDA, and *p*-PDA, respectively. These ions were consistent with the molecular formulas $(C_{12}H_{11}O_2N_2)^+$, $(C_{12}H_{11}N_4)^+$, and $(C_{18}H_{19}N_6)^+$. These ions are consistent with the protonated forms of the oxidation products of the amines as shown below. Also, these analyses are consistent with values found elsewhere.[91,97,107] However, the oxidative condensation process involves a 4e oxidation for *o*-AP to produce 2-amino-phenoxazin-3-ol (APZ). But, a 6e oxidation is apparent for the oxidation of *o*-PDA and *p*-PDA to obtain 2,3-diaminophenazine (DAP) and 2,2′-diaminoazabenzene (AB), respectively.

Generally, the first 2e oxidation is a result of the reduction of the metal complexes.[93,108] This means that 2 equiv of the metal complexes is initially reduced by 1 equiv of the various amines. Since the benzoquinone imines are established to react with another molecule of the amines to afford the dimeric or trimeric oxidation products, the oxidation products are expected to be as follows:[108]

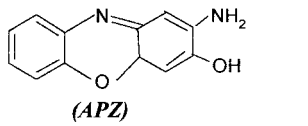

(APZ)

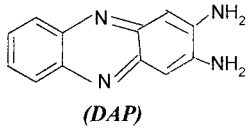

(DAP)

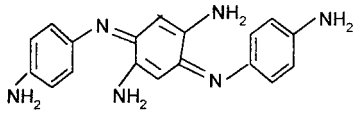

(AB)

The experimental results indicate that the redox reaction between the amines and the immobilized metal complexes on H_ISiO_2 follows an *outer-sphere* mechanism.[109,110] The postulated mechanism is described as follows, where L = H_2O, R = propyl group, A = amines, and S = H_ISiO_2 support.

$$[S-(RNH_2)_2ML_2]^{n+} + A \underset{k_{-1}}{\overset{k_1}{\rightleftharpoons}} \{[S-(RNH_2)_2ML_2]^{n+}\cdots A\} \quad (1)$$

(formation of the counterion pair)

$$\{[S-(RNH_2)_2ML_2]^{n+}\cdots A\} \underset{k_{-2}}{\overset{k_2}{\rightleftharpoons}} \{[S-(RNH_2)_2ML_2]-A\}^{n+} \quad (2)$$

(restructuring of the encounter complex to set up the electron transfer)

$$\{[S-(RNH_2)_2ML_2]-A\}^{n+} \xrightarrow[\text{slow}]{k_3} [S-(RNH_2)_2ML_2]^{n-1} + A^+ \xrightarrow[\text{fast}]{k_4} \text{oxidation product} \quad (3)$$

$$dx/dt = k_3\{[S-(RNH_2)_2ML_2]-A\}^{n+} \quad (4)$$

Applying the steady-state approximation principle

$$[\{[S-(RNH_2)_2ML_2]-A\}^{n+}]/dt = k_2[\{[S-(RNH_2)_2ML_2]^{n+}\cdots A\}] - k_{-2}[\{[S-(RNH_2)_2ML_2]-A\}^{n+}] - k_3[\{[S-(RNH_2)_2ML_2]-A\}^{n+}] = 0 \quad (5)$$

$$[\{[S-(RNH_2)_2ML_2]-A\}^{n+}] = \frac{k_2[\{[S-(RNH_2)_2ML_2]^{n+}\cdots A\}]}{k_3 + k_{-2}} \quad (6)$$

$$dx/dt = \frac{k_2k_3K_1[A][[S-(RNH_2)_2ML_2]^{n+}]}{k_3 + k_{-2}} \quad (7)$$

Applying a preequilibrium approximation

$$dx/dt = k_3K_1K_2[A][[S-(RNH_2)_2ML_2]^{n+}] \quad (8)$$

where $K_1 = k_1/k_{-1}$ and $K_2 = k_2/k_{-2}$.

The rate eq 7 confirms that the rate of the redox reaction is proportional to $[[S-(RNH_2)_2ML_2]^{n+}]$ and [amine]. This means that the reaction shows first-order kinetics for [amine] in the heterogeneous system.

Conclusion

Our approach for the preparation of H_lSiO_2 using the Attard route has been performed with some modification of the procedure according to the nature of the surfactant. The resulting silica materials have opened new opportunities in various applicable fields, particularly in the study of the kinetics of redox reactions. The high concentration of nonionic surfactant leads to a well-resolved monolithic glassy material. The mechanism of the generation of H_lSiO_2 occurs via a real liquid crystal template. Therefore, the silica framework composition can easily be modified by an aminosilane and then incorporated with metal complexes.

The kinetic studies of the amine oxidation by the incorporated mesoporous metal complexes show clearly that (i) the redox reaction obeys first-order kinetics, (ii) the redox reaction between amines and complexes **III** and **IV** exhibits an apparent induction period independent of the temperature, (iii) the induction time is inversly proportional to the concentration and reactivity of the amines, and (iv) all the kinetic results show that the outer-sphere mechanism is dominant in this redox reaction.

Acknowledgment. We are indebted to S. Fiddy for providing helpful and related fruitful discussion, T. Cambell for important assistance, S. Turin for help with IR spectroscopy, the groups of Professors G. R. Luckhurst and M. T. Weller for help with EPR and PXRD studies, respectively, M. Salam and M. Ghanim for their continuous encouragement, and also the Egyptian Government for financial support.

References and Notes

(1) Pendyala, L.; Kidani, Y.; Perez, R.; Wilkes, J.; Creaven, J. P. *Cancer Lett.* **1995**, *97*, 177.
(2) Behrens, B. C.; Hamilton, T. C.; Masuda, H.; Gratzinger, K. R.; Peng, J. W.; Louic, K. G.; Knutsen, T.; McKay, W. M. *Cancer Res.* **1987**, *47*, 414.
(3) Lippard, S. J.; Bond, P. J.; Wu, K. C.; Bauer, R. *Science* **1976**, *194*, 726.
(4) Roszak, A. W.; Clement, O.; Buncel, E. *Acta Crystallogr., Sect. C* **1996**, *52*, 1645.
(5) Maeder, M.; Macke, H. *Inorg. Chem.* **1994**, *33*, 3135.
(6) Goto, M.; Kanda, N.; Sakai, T.; Goedken, V. *Inorg. Chem.* **1985**, *24*, 582.
(7) Goedken, V. *J. Chem. Soc., Chem. Commun.* **1972**, 207.
(8) Olsen, C. D.; Vasilevskis, J. *Inorg. Chem.* **1971**, *10*, 463.
(9) Barefield, E. K.; Mocella, T. M. *J. Am. Chem. Soc.* **1975**, *97*, 4238.
(10) Curtis, N. F. *J. Chem. Soc. A* **1971**, 2834.
(11) Ridd, J. M.; Keene, R. F. *J. Am. Chem. Soc.* **1981**, *103*, 5733.
(12) Miller, D. J.; Watts, B. J.; Waddan, Y. D. *Inorg. Chim. Acta* **1975**, *12*, 267.
(13) Schwarz, F.; Scholhorn, H.; Thewalt, U.; Lippert, B. *J. Chem. Soc., Chem. Commun.* **1993**, 1282.
(14) Simandi, L. I. *Int. Rev. Phys. Chem.* **1989**, *8*, 21.
(15) Simandi, L. I.; Barna, T.; Nemeth, S. *J. Chem. Soc., Dalton Trans.* **1996**, 473.
(16) Iseminger, P. W.; Gregory, M.; Timothy, J. R.; Caple, G.; Sykes, A. G. *J. Org. Chem.* **1997**, *62*, 2643.
(17) Hollstein, U. *Chem. Rev.* **1974**, *74*, 625.
(18) Katz, E.; Weissbach, H. *J. Biol. Chem.* **1962**, *237*, 882.
(19) Frei, E. *Cancer Chemother. Rep.* **1974**, *58*, 49.
(20) Nickel, U.; Ruehl, N.; Zhou, B. M. *Z. Phys. Chem.* **1986**, *148*, 33.
(21) Ignaczak M.; Dziegiec, J. *Kinet. Katal.* **1989**, *30*, 1026.
(22) Ignaczak, M.; Dziegiec, J.; Leszczynski, L. *Pol. J. Chem.* **1990**, *64*, 21.
(23) Ramachandran, M. S.; Vivekanadam, T. S.; Subbaratnam, N. R.; Rajaram, N. *Indian J. Chem.* **1983**, *22A*, 895.
(24) Barry, C. E.; Nayar, P. G.; Begley, T. P. *Biochemistry* **1988**, *28*, 6323.
(25) Yano, Y.; Ikuta, M.; Amamiya, Y.; Nabeshima, T. *Chem. Lett.* **1991**, 461.
(26) Krylov, V. K.; Bavina, M. V.; Kukushkin, Y. N. *J. Appl. Chem. USSR* **1992**, *65* (9), 1622.
(27) Josehine, O.; Ehighaorkhuo, J.; Folorunso, O.; Olusegun, O. *J. Chem. Soc., Dalton Trans.* **1985**, 1665.
(28) Kresge, C. T.; Leonowicz, M. E.; Roth, W. J.; Vartuli, J. C.; Beck, J. S. *Nature* **1992**, *359*, 710.
(29) Beck, J. S.; Vartuli, J. C.; Roth, W. J.; Leonowicz, M. E.; Kresge, T. C.; Schmitt, K. D.; Chu, C. T. W.; Olsan, D. H.; Higgins, E. W.; Schlenker, J. L. *J. Am. Chem. Soc.* **1992**, *114*, 10834.
(30) Yanagisawa, Y.; Shimizu, T.; Kurota, K.; Kato, C. *Bull. Chem. Soc. Jpn.* **1990**, *63*, 988.
(31) Inagaki, S.; Fukushima, Y.; Kuroda, K. *J. Chem. Soc., Chem. Commun.* **1993**, 680.
(32) Inagaki, S.; Koiwai, A.; Suzuki, N.; Fukushima, Y.; Kuroda, K. *Bull. Chem. Soc. Jpn.* **1996**, *69*, 1449.
(33) Armengal, E.; Corma, A.; Garcia, H.; Primo, J. *Appl. Catal., A* **1995**, *149*, 411.
(34) Gunnewgh, E. A.; Gopie, S. S.; VanBekkum, H. *J. Mol. Catal., A* **1996**, *106*, 151.
(35) Climent, M. J.; Corma, A.; Lopez, R.; Iborra, S.; Primo, J. *J. Catal.* **1998**, *175*, 70.
(36) Canva, M.; Georges, P.; Pereligritz, F. J.; Brum, A.; Chaput, A. *Appl. Opt.* **1995**, *34*, 428.
(37) Wei, Y.; Yeh, M. J.; Jin, D.; Jia, X.; Wang, J. *Chem. Mater.* **1995**, *7*, 969.
(38) Chum, W. G.; Thomas, B. *Science* **1994**, *266*, 1013.
(39) Chum, W. G.; Thomas, B. *Science* **1994**, *264*, 1757.
(40) O'Brien, S.; Francis, J. R.; Prices, J. S.; Clark, M. S.; Okazaki, N.; Kuroda, K. *J. Chem. Soc., Chem. Commun.* **1995**, 2423.
(41) Huo, K.; Morgalese, L. D.; Cies, P. F.; Gier, E. T.; Sieger, P.; Leon, R.; Petroff, M. P.; Schuth, F.; Stucky, G. D. *Nature* **1994**, *368*, 317.
(42) Huo, Q.; Margolese, L. D.; Stucky, G. D. *Chem. Mater.* **1996**, *8*, 1147.
(43) Bagshaw, A. S.; Pruzet, E.; Pinnavaia, T. J. *Science* **1995**, *269*, 1242.
(44) Bagshaw, A. S.; Pinnavaia, T. J. *Angew. Chem., Int. Ed. Engl.* **1996**, *35*, 1102.
(45) Prouzet, E.; Pinnavaia, T. J. *Angew. Chem., Int. Ed. Engl.* **1997**, *36*, 516.
(46) Voegtlin, C. A.; Ruch, F.; Guth, L. J.; Patarin, J.; Huve, L. *Microporous Mater.* **1997**, *9*, 95.
(47) Mercier, L.; Pinnavaia, T. J. *Adv. Mater.* **1997**, *9*, 500.
(48) Braun, V. P.; Osenar, P.; Stupp, L. S. *Nature* **1996**, *380*, 325.
(49) Attard, G. S.; Glyde, J. C.; Göltner, C. G. *Nature* **1995**, *378*, 366.
(50) Leal, O.; Anderson, D. L.; Bowman, R. C.; Basolo, F.; Burwell, R. L. *J. Am. Chem. Soc.* **1975**, *97*, 5125.
(51) Haller, I. *J. Am. Chem. Soc.* **1978**, *100*, 8050.
(52) Hernan, P.; Pino, C.; Huitzky, E. R. *Chem. Mater.* **1992**, *4*, 49.
(53) Miki, K.; Sato, Y. *Bull. Chem. Soc. Jpn.* **1993**, *66*, 2385.
(54) Pugin, B.; Müller, M. *Stud. Surf. Sci. Catal.* **1993**, *78*, 107.
(55) Beharinger, K. D.; Blümel, J. *Chem. Commun.* **1996**, 653.
(56) Cauvel, A.; Renord, G.; Brunel, D. *J. Org. Chem.* **1997**, *62*, 749.
(57) Brunel, D.; Cauvel, A.; Fajula, F.; DiRenzo, F. *Stud. Surf. Sci. Catal.* **1995**, *97*, 173.
(58) Sutra, P.; Brunel, D. *Chem. Commun.* **1996**, 2485.
(59) Diaz, F. J.; Balkus, J. K.; Bedioui, F.; Kurshev, V.; Kevan, L. *Chem. Mater.* **1997**, *9*, 61.
(60) Kimura, T.; Saeki, S.; Sagahara, Y.; Kuroda, K. *Langmuir* **1998**, *15*, 2794.
(61) James, G. E.; James, C. H.; Macquarrie, D. J. *Synlett* **1998**, 625.
(62) Ryoo, R.; Kim, J. M. *J. Chem. Soc., Chem. Commun.* **1995**, 711.
(63) Braun, P. V.; Osenar, P.; Stupp, S. I. *Nature* **1996**, *380*, 325.
(64) Attard, G. S.; Edgar, M.; Göltner, C. G. *Acta Mater.* **1998**, *46*, 751.
(65) Yang, H.; Ovk, G.; Coombs, N.; Sokolov, I.; Ozin, G. A. *J. Mater. Chem.* **1998**, *8*, 743.
(66) Gregg, S. J.; Sing, K. S. *Adsorption, Surface Area and Porosity*, 2nd ed.; Academic Press: London, 1992.
(67) Wei, D.; Wang, H.; Feng, X.; Chuch, W.; Ravikovitch, P.; Lyubovsky, M.; Li, C.; Takeguchi, T.; Haller, G. L. *J. Phys. Chem. B* **1999**, *103*, 2113.
(68) Firauzi, A.; Atef, F.; Oertli, A. G.; Stucky, G. D.; Chmekia, B. F. *J. Am. Chem. Soc.* **1997**, *119*, 3596.
(69) Chem, C. Y.; Li, X. H.; Davis, M. E. *Microporous Mater.* **1993**, *2*, 27.

(70) Burkett, S. L.; Sims, S. D.; Mann, S. *Chem. Commun.* **1996**, 1367.
(71) Prakash, A. M.; Hartmann, M.; Kevan, L. *J. Phys. Chem. B* **1997**, *101*, 6819.
(72) Engelhardt, G.; Michel, D. *High-Resolution Solid State NMR of Silicates and Zeolites*; Wiley: New York, **1987**.
(73) Sindorf, D. W.; Maciel, G. E. *J. Am. Chem. Soc.* **1983**, *105*, 3769.
(74) Feng, X.; Fryxell, G. E.; Wang, L. Q.; Kim, A. Y.; Liu, J.; Kemner, K. M. *Science* **1997**, *276*, 923.
(75) Impens, N. R.; Voort, P. V.; Vansant, E. F. *Microporous Mesoporous Mater.* **1999**, *28*, 217.
(76) Kim, G. J.; Kim, S. H. *Catal. Lett.* **1999**, *57*, 139.
(77) Liu, C. J.; Li, S. G.; Pang, V. Q.; Che, C. M. *Chem. Commun.* **1997**, 65.
(78) Liu, C. J.; Yu, W. Y.; Li, S. G.; Che, C. M. *J. Org. Chem.* **1998**, *63*, 7364.
(79) Geschwind, S.; Kisliuk, M. P.; Remeika, J. P.; Wood, D. L. *Phys. Rev.* **1962**, *126*, 1684.
(80) McClure, D. S. *J. Chem. Phys.* **1962**, *36*, 2757.
(81) Park, D. H.; Park, S. S.; Choe, S. J. *Bull. Korean Chem. Soc.* **1999**, *20*, 291.
(82) Xu, J.; Luan, Z.; Wasowicz, T.; Kevan, L. *Microporous Mesoporous Mater.* **1998**, *22*, 179.
(83) Goldforb, D. *Zeolites* **1989**, *9*, 509.
(84) Goldberg, D. P.; et al. *J. Am. Chem. Soc.* **1997**, *119*, 8722.
(85) Wekhuysen, B. L.; Schoonheydt, R. A. *J. Phys. Chem. B* **1997**, *101*, 309.
(86) Luan, Z.; Xu, J.; Kevan, H. *Chem. Mater.* **1998**, *10*, 3699.
(87) Kurshev, V.; Kevan, L.; Parillo, D. J.; Kokatailo, G. T.; Gorte, R. *J. Phys. Chem.* **1994**, *98*, 10160.
(88) Karthein, R.; Motschi, H.; Schweiger, A.; Ibric, S.; Sulzberger, B.; Stumm, W. *Inorg. Chem.* **1991**, *30*, 1606.
(89) Giamello, E.; Murphy, D.; Magnacca, G.; Marterra, C.; Shioya, V.; Nomura, T.; Anpo, M. *J. Catal.* **1992**, *136*, 510.
(90) Huang, H.; Cai, R.; Du, Y.; Lin, Z.; Zeng, Y. *Anal. Chim. Acta* **1995**, *318*, 63.
(91) Szeverenyi, Z.; Milaeva, E. R.; Simandi, L. I. *J. Mol. Catal.* **1991**, *67*, 251.
(92) Perezuiz, T.; Martinez, C.; Tomas, V.; Corrion, F. J. *Int. J. Environ. Anal. Chem.* **1993**, *53*, 195.
(93) Takashi, N.; Tadanori, H.; Masakazu, Y.; Hiroshi, M.; Yasuhiko, S. *Bull. Chem. Soc. Jpn.* **1975**, *48*, 3709.
(94) Davies, C. W.; Thomas, G. G. *J. Chem. Soc.* **1952**, 1607.
(95) Mambo, E.; Simoyi, R. H. *J. Phys. Chem.* **1993**, *79*, 13662.
(96) Berglund, J.; Fronaeus, S.; Elding, L. I. *Inorg. Chem.* **1993**, *32*, 4527.
(97) Zaki, A. B.; El-Sheikh, M. Y.; Evans, J.; El-Safty, S. A. *Polyhedron* **2000**, *19*, 1317.
(98) Shriver, D. F.; Atkins, P. W.; Langford, C. H. *Inorganic Chemistry*; Oxford University Press: London, 1990.
(99) Pearson, R. G. *J. Chem. Phys.* **1952**, *20*, 1478.
(100) Kushik, R. D.; Joshi, D. R.; Kumari, S. *Asian J. Chem.* **1998**, *10*, 573.
(101) Helferich, F. *Ion Exchange*; Mc-Graw-Hill Book Co.: New York, 1962.
(102) Bänsch, B.; Martinez, P.; Uribe, D.; Zuluaga, J.; Van Eldik, R. *Inorg. Chem.* **1991**, *30*, 4555.
(103) El-Sheikh, M. Y.; Habib, A. M.; Ashmawy, F. M.; Gemeay, A. H.; Zaki, A. B. *Transition Met. Chem. (Dordrecht, Neth.)* **1989**, *14*, 95.
(104) Purcell, K. F.; Katz, J. C. *Inorganic Chemistry*; W. B. Saunders: London, 1977.
(105) Griffith, W. P. In *The Chemistry of the Rarer Platinum Metals*; Wiley Interscience: London, 1967.
(106) Laidler, K. L. *Chemical Kinetics*; T. M. H. Publishing Co. Ltd.: New Delhi, 1977.
(107) Yano, Y.; Ikuta, M.; Amamiya, Y.; Nabeshima, T. *Chem. Lett.* **1991**, 461.
(108) Zhu, Y.; Li, J.; Liu, Z.; Cheng, G.; Dong, S.; Wang, E. *J. Mol. Catal., B Enzymatic* **1998**, *4*, 33.
(109) Rosseinsky, D. R. *Chem. Rev.* **1972**, *72*, 215.
(110) Hubig, S. M.; Rathore, R.; Kochi, J. K. *J. Am. Chem. Soc.* **1999**, *121*, 617.